

Article

Synthesis, Characterization and Study of Liquid Crystals Based on the Ionic Association of the Keplerate Anion $[\text{Mo}_{132}\text{O}_{372}(\text{CH}_3\text{COO})_{30}(\text{H}_2\text{O})_{72}]^{42-}$ and Imidazolium Cations

Nancy Watfa ^{1,2,3}, Sébastien Floquet ^{1,*}, Emmanuel Terazzi ⁴, William Salomon ¹, Laure Guénée ⁴, Kerry Lee Buchwalder ⁴, Akram Hijazi ^{2,3}, Daoud Naoufal ^{2,3}, Claude Piguet ⁴ and Emmanuel Cadot ¹

¹ Institut Lavoisier de Versailles, UMR 8180, University of Versailles, 45 avenue des Etats-Unis, Versailles 78035, France; E-Mails: nancy_watfa87@hotmail.com (N.W.); william.salomon@uvsq.fr (W.S.); emmanuel.cadot@uvsq.fr (E.C.)

² Laboratoire de Chimie de Coordination Inorganique et Organométallique LCIO, Université Libanaise, Faculté des Sciences I, Hadath, Lebanon; E-Mails: hijazi_akram@hotmail.com (A.H.); dnaoufal@ul.edu.lb (D.N.)

³ Ecole Doctorale des Sciences et Technologie EDST, PRASE, Université Libanaise, Hadath, Lebanon

⁴ Department of Inorganic and Analytical Chemistry, University of Geneva, 30 quai E. Ansermet, Geneva CH-1211, Switzerland; E-Mails: Emmanuel.Terazzi@unige.ch (E.T.); Laure.Guenee@unige.ch (L.G.); Kerry.Buchwalder@unige.ch (K.L.B.); Claude.Piguet@unige.ch (C.P.)

* Author to whom correspondence should be addressed; E-Mail: sebastien.floquet@uvsq.fr; Tel.: +33-139254379; Fax: +33-139254452.

Academic Editors: Greta Ricarda Patzke and Pierre-Emmanuel Car

Received: 21 April 2015 / Accepted: 20 May 2015 / Published: 5 June 2015

Abstract: A series of eight new materials based on the ionic association between 1-methyl-3-alkylimidazolium cations and the nanometric anionic Keplerate $[\text{Mo}_{132}\text{O}_{372}(\text{CH}_3\text{COO})_{30}(\text{H}_2\text{O})_{72}]^{42-}$ has been prepared and characterized in the solid state. The liquid crystal properties of these materials were investigated by the combination of Polarized Optical Microscopy, Differential Scanning Calorimetry and Small-angle X-Ray Diffraction showing a self-organization in lamellar (L) mesophases for the major part of them. From the interlamellar spacing h and the intercluster distance a_{hex} , we demonstrated that the cations are not randomly organized around the anionic cluster and that the alkyl

chains of the cations are certainly folded, which limits the van der Waals interactions between the cations within the liquid crystal phase and therefore harms the quality of the mesophases.

Keywords: polyoxometalates; Keplerate; cluster; liquid crystal

1. Introduction

Liquid crystals constitute a fascinating example of functional self-assembled materials. Incorporation of some inorganic components into liquid crystalline phases appears particularly relevant to the elaboration of synergistic multifunctional materials according to a “bottom-up” approach [1]. Polyoxometalates (POMs), often described as polyanionic molecular oxides, exhibit various properties in all domains of chemistry [2–8]. Dietz and Wu demonstrated that the association of various POMs with phosphonium or ammonium derivatives lead to ionic liquids or ionic mesomorphic self-assemblies [9–17]. In this context, the “Keplerates” anions with the general formula $[(\text{Mo}_6\text{O}_{21})_{12}(\text{linker})_{30}(\text{Ligand})_{30}(\text{H}_2\text{O})_{72}]^{n-}$ (Figure 1) constitute a unique class of nanoscopic hollow spherical clusters which exhibit singular structural features which easily exchange the internal ligands/functionalities [18,19]. They therefore constitute a fascinating class of molecular materials which display a large variety of properties such as magnetism [20,21], catalysis [22,23], electric conductivity [24], non-linear optics [25,26] and are able to serve as nano-reactor for chemical reactions, such as stoichiometric transformations of substrates with unusual selectivity [27]. Several research groups have been interested to exploit this cluster in the context of materials science where many efforts have been done to organize and stabilize such materials. For example, the incorporation of Keplerates into suitable matrices such as polymers [28] polyelectrolyte [29] silica [30] or organic cations [31–34] can enhance stability and induce synergistic functionalities between POMs and matrices. For instance, the counter-cations of the Keplerate anion $[\text{Mo}_{132}\text{O}_{372}(\text{CH}_3\text{COO})_{30}(\text{H}_2\text{O})_{72}]^{42-}$, noted hereafter Mo_{132} , can be replaced with dioctadecyl-dimethylammonium cations (DODA^+) resulting in functional nanodevices [35]. Motivated by this challenge, we reported that the wrapping of Keplerate-type capsules with DODA^+ cations lead to the formation of the materials $(\text{DODA})_{36}(\text{NH}_4)_6[\text{Mo}_{132}\text{O}_{372}(\text{CH}_3\text{COO})_{30}(\text{H}_2\text{O})_{72}] \cdot 75\text{H}_2\text{O}$, $(\text{DODA})_{44}(\text{NH}_4)_{14}[\text{Mo}_{132}\text{O}_{312}\text{S}_{60}(\text{SO}_4)_{23}(\text{H}_2\text{O})_{86}]$ and $(\text{DODA})_{56}(\text{NH}_4)_{16}[\text{Mo}_{132}\text{O}_{312}\text{S}_{60}(\text{SO}_4)_{30}(\text{H}_2\text{O})_{72}]$ which exhibit liquid crystalline properties [36,37]. Interestingly, the DODA^+ cations are not randomly distributed on the surface of the Keplerate capsule, but organized within the sheets of Keplerates. In the following of these two previous works, we studied the association of another highly charged POM, namely $[\text{K}_2\text{Na}_x\text{Li}_y\text{H}_z\{\text{Mo}_4\text{O}_4\text{S}_4(\text{OH})_2(\text{H}_2\text{O})_3\}_2(\text{P}_8\text{W}_{48}\text{O}_{184})]^{(34-x-y-z)-}$ with a series of 1-methyl-3-alkylimidazolium cations [38], which present the particularities to be easily modified and to be easily prepared on a gram scale. This work evidenced that the chains of the cations are organized perpendicularly to the sheets of the POMs and that the structural parameters of the liquid crystal phases can be finely tuned as a function of the alkyl chain length of the imidazolium cations [38]. More recently, we evidenced that the Keplerate Mo_{132} interacts with 1-methyl-3-ethylimidazolium

cations in aqueous phase with an association constant of 5800, a value significantly higher than that measured with tetramethylammonium cation (1550) taken as a model for the DODA⁺ cation [39].

We report here on the synthesis and the characterizations of materials built from the ionic association of Keplerate Mo₁₃₂ with 1-methyl-3-alkylimidazolium cations, noted mimC_n⁺ (n = 12, 14, 16, 18, 20, see Figure 1). After having characterized the materials, the liquid crystal properties are studied by polarized optical microscopy (TD-POM), differential scanning calorimetry (DSC) and small angle variable temperature X-ray diffraction (SA-XRD) in order to determine if it is possible (i) to build liquid crystals materials resulting from the ionic associations Mo₁₃₂ / 1-methyl-3-alkylimidazolium and (ii) to change the nature of the liquid crystal phases upon replacement of DODA⁺ cations with 1-methyl-3-alkylimidazolium cations, for which the interaction with Mo₁₃₂ is stronger in solution.

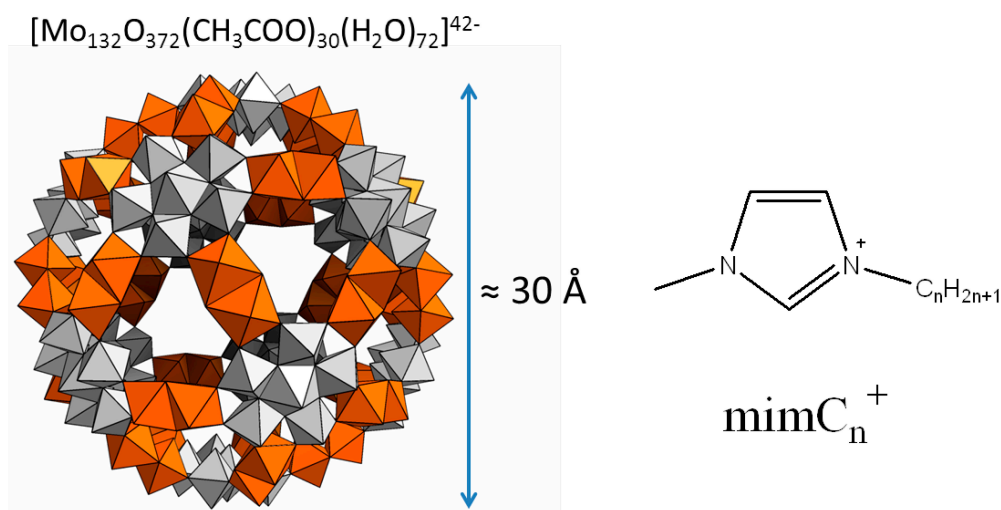


Figure 1. Representation of the Keplerate nano capsule Mo₁₃₂ and the imidazolium cations used in this study. The grey polyhedra correspond to the fragments {Mo₆O₂₁}, whereas the polyhedra in orange correspond to the linkers {Mo₂O₄}. Acetates ligands are found inside the cavity of the capsule and are not shown in the figure.

2. Results and Discussion

2.1. Synthesis and Characterization of the Mo₁₃₂-Based Materials

2.1.1. Synthesis and Characterizations

The Keplerate-based materials were prepared by mixing an aqueous solution of the precursor compound abbreviated NH₄-Mo₁₃₂ with a large excess (*ca.* 170 equivalents per Mo₁₃₂ capsule) of 1-methyl-3-alkylimidazolium cations, noted mimC_n⁺ (n = 12, 14, 16, 18, 20), in chloroform in order to replace the maximum of NH₄⁺ counteranions. After stirring the mixture for about 1 h, the Keplerate capsule Mo₁₃₂ was totally transferred into the chloroform phase, indicating a rapid and quantitative transfer. The target materials were precipitated with a good yield by addition of ethanol into the chloroform phase and finally filtered, washed with ethanol and dried in air (see experimental section for more details). We were also interested to investigate the preparation of mixed salts of mimC₁₂⁺ and mimC₂₀⁺ by using different ratios during the synthesis. The materials were obtained as

brown-black soft solids, no longer soluble in water, but soluble in organic solvents such as chloroform, acetonitrile, toluene and ether. These compounds were characterized by FT-IR, TGA, EDX and elemental analyses.

FT-IR spectra were performed using Diamond ATR technique and an ATR correction was applied. As shown in Figure 2 for the compound (mimC₁₈)₃₇-Mo₁₃₂, the comparison of its IR spectrum with those of the precursors confirm the conservation of the Mo₁₃₂ cluster and its association with the organic cation since the IR-spectrum exhibits the characteristic bands of both components. In addition the band at 1403 cm⁻¹, attributed to NH₄⁺ counter-cations, is still present in the final material indicating that not all NH₄⁺ have been replaced by the organic cations in agreement with previous studies [36,37].

Based on the data of the elemental analyses (C, H, N, Mo), EDX and TGA, the structural formula of the obtained materials is established. The results are summarized in Table 1 and more details are available in the experimental section. Firstly, EDX measurements evidence only the presence of the Mo and reveal the absence of Bromide ions, the fingerprint of the presence of the starting imidazolium salt. The number of acetate ligands was 30 for all synthesized compound. It should be noted that, despite the large excess of the organic cations, the replacement of the ammonium cations was not complete, in agreement with FT-IR spectra. The number of interacting organic cations with the Keplerate ion was found between 36 and 41, which is consistent with the previously published result with DODA salts [36,37]. This result suggests that some NH₄⁺ are probably trapped within the Mo₁₃₂ nanocapsule. It is worth noting that by mixing imidazolium salts bearing C₁₂ and C₂₀ alkyl chains, a purely statistical distribution is observed in the final compound where the number of each organic cations is controlled with the initial ratio. This demonstrates the possibility to tune the final composition of the mixed surfactant encapsulated clusters, a key parameter for the design of functional materials. Finally, the thermogravimetric analyses estimate the total amount of water molecules.

Table 1. Molecular formula of the Mo₁₃₂-based materials established from elemental analysis and TGA.

Samples	Estimated Molecular Formula
(mimC ₁₂) ₃₆ -Mo ₁₃₂	(mimC ₁₂ H ₂₅) ₃₆ (NH ₄) ₆ [Mo ₁₃₂ O ₃₇₂ (CH ₃ COO) ₃₀ (H ₂ O) ₇₂].38H ₂ O
(mimC ₁₄) ₃₈ -Mo ₁₃₂	(mimC ₁₄ H ₂₉) ₃₈ (NH ₄) ₄ [Mo ₁₃₂ O ₃₇₂ (CH ₃ COO) ₃₀ (H ₂ O) ₇₂].30H ₂ O
(mimC ₁₆) ₄₁ -Mo ₁₃₂	(mimC ₁₆ H ₃₃) ₄₁ (NH ₄) ₁ [Mo ₁₃₂ O ₃₇₂ (CH ₃ COO) ₃₀ (H ₂ O) ₇₂].38H ₂ O
(mimC ₁₈) ₃₇ -Mo ₁₃₂	(mimC ₁₈ H ₃₇) ₃₇ (NH ₄) ₅ [Mo ₁₃₂ O ₃₇₂ (CH ₃ COO) ₃₀ (H ₂ O) ₇₂].48H ₂ O
(mimC ₂₀) ₃₇ -Mo ₁₃₂	(mimC ₂₀ H ₄₁) ₃₇ (NH ₄) ₅ [Mo ₁₃₂ O ₃₇₂ (CH ₃ COO) ₃₀ (H ₂ O) ₇₂].43H ₂ O
(mimC ₁₂) ₂₀ (mimC ₂₀) ₂₀ -Mo ₁₃₂	(mimC ₁₂ H ₂₅) ₂₀ (mimC ₂₀ H ₃₃) ₂₀ (NH ₄) ₂ [Mo ₁₃₂ O ₃₇₂ (CH ₃ COO) ₃₀ (H ₂ O) ₇₂].38H ₂ O
(mimC ₁₂) ₃₃ (mimC ₂₀) ₇ -Mo ₁₃₂	(mimC ₁₂ H ₂₅) ₃₃ (mimC ₂₀ H ₃₃) ₇ (NH ₄) ₂ [Mo ₁₃₂ O ₃₇₂ (CH ₃ COO) ₃₀ (H ₂ O) ₇₂].48H ₂ O
(mimC ₁₂) ₈ (mimC ₂₀) ₃₃ -Mo ₁₃₂	(mimC ₁₂ H ₂₅) ₈ (mimC ₂₀ H ₃₃) ₃₃ (NH ₄) ₁ [Mo ₁₃₂ O ₃₇₂ (CH ₃ COO) ₃₀ (H ₂ O) ₇₂].38H ₂ O

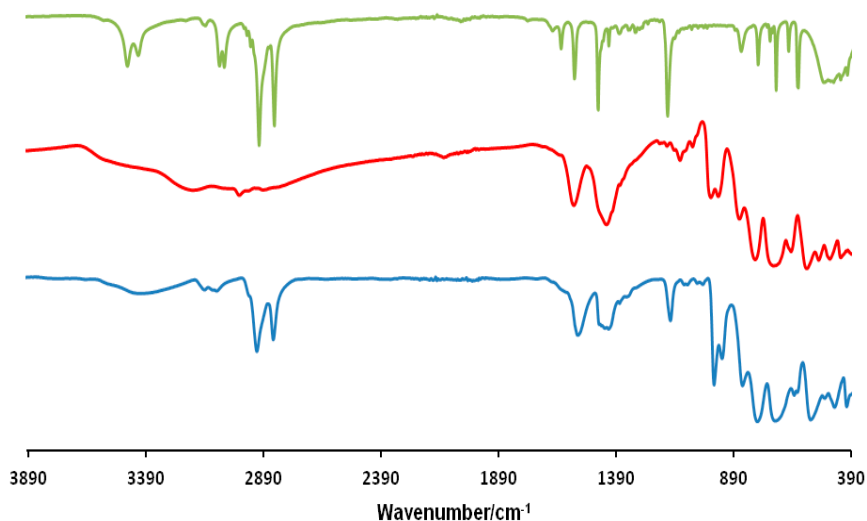


Figure 2. FT-IR spectra of (mimC₁₈)Br (**green**), NH₄-Mo₁₃₂ (**red**) and (mimC₁₈)₃₇-Mo₁₃₂ (**blue**).

2.1.2. Thermal Stability of the Mo₁₃₂-Based Materials

Chemical stability of the Mo₁₃₂-based materials was assessed by TGA under N₂ and O₂ and FT-IR measurements at variable temperature under N₂ and under O₂. TGA traces recorded under oxygen display a first stage between 20 °C and 180 °C corresponding to the removal of all the water molecules (hydration and coordination) followed by a large weight loss in the 250–800 °C temperature range, which is assigned to the decomposition of the cations and of the acetate ligands of the Mo₁₃₂ cluster to give molybdenum oxides. This second step translates into a thermal stability of about 250 °C for our Mo₁₃₂-based materials.

Variable temperature FT-IR studies were performed on the compound (mimC₁₈)₃₇-Mo₁₃₂ arbitrarily chosen as a reference compound. The FT-IR spectra were recorded in diffuse reflectance mode on a sample of (mimC₁₈)₃₇Mo₁₃₂ dispersed into a KBr matrix. The experiments were done either under air or under a flow of nitrogen between 20 °C and 400 °C with a heating/cooling rate of 2 °C/min. The results obtained under air atmosphere are shown in Figure 3 for different temperatures. In these conditions, the disappearance of the bands characteristic of the water molecules around 3400 cm⁻¹ and 1640 cm⁻¹ below 180 °C agrees with TGA. If we focus on the vibration bands assigned to the Keplerate capsules in the 1000–400 cm⁻¹ range, no significant modification are observed up to ≈125 °C. In contrast, dramatic changes are observed between 125 °C and 200 °C, especially for the strong bands located at 855, 727 and 574 cm⁻¹, which almost totally disappear, while the two bands assigned to the Mo=O stretching vibration located at 975 and 939 cm⁻¹ give only one strong band at 953 cm⁻¹ at 190 °C. Concomitantly, the color of the compound turns to blue and this phenomenon is not reversible upon returning room temperature, which indicates that the Keplerate capsule in the compound (mimC₁₈)₃₇Mo₁₃₂ is not stable in air above 125 °C.

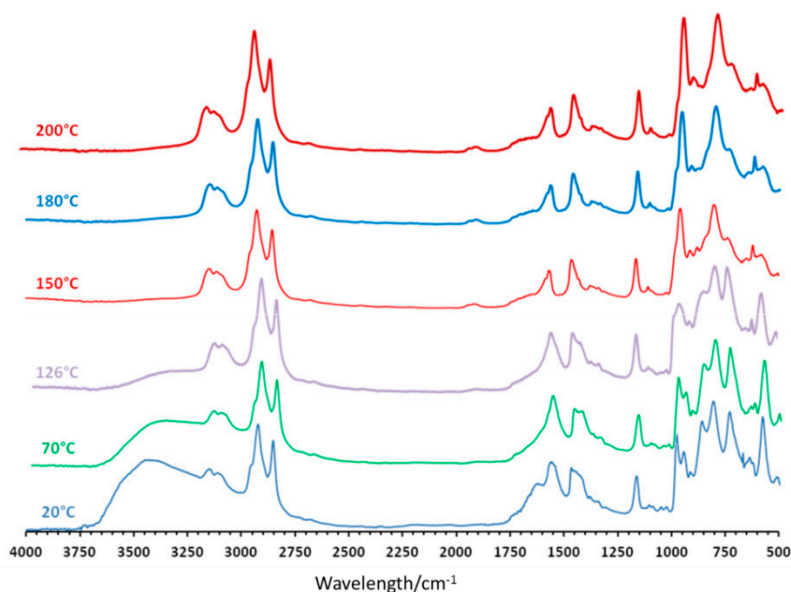


Figure 3. Selected FT-IR spectra recorded at various temperatures for compound $(\text{mimC}_{18})_{37}\{\text{Mo}_{132}\}$ under air.

Similar experiments were performed under a flow of nitrogen and the results obtained under nitrogen are shown in Figure 4. In these conditions, the behavior is totally different. The removal of water molecules is observed between 20 °C and 180 °C, but only small changes in the Keplerate skeleton are observed on the FT-IR spectra, in contrast with experiment performed in air. From 20 °C to 250 °C, the main evolution observed concerns the vibration band at 855 cm^{-1} , for which the intensity decreases with increasing temperature, but this modification is reversible when returning room temperature after re-hydration of the material. Finally, heating the compound at temperature higher than 250 °C provokes the degradation of the organic cation and of the acetate ligands in agreement with TGA. This is associated with a strong modification of the Keplerate.

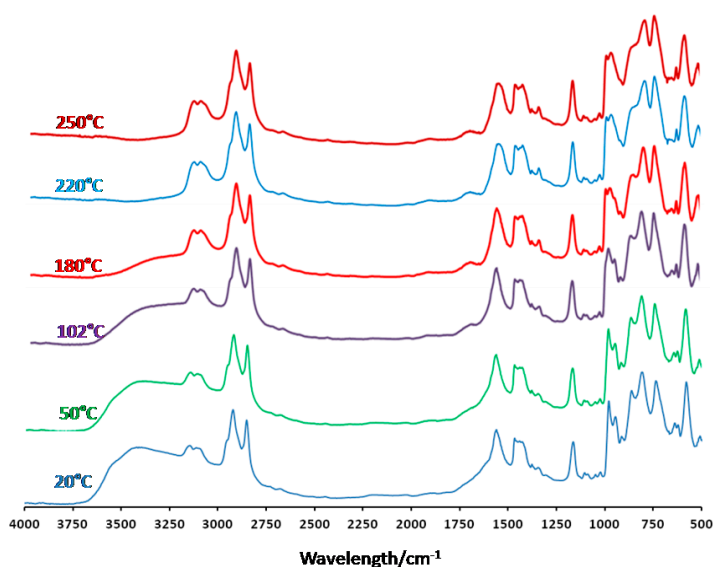


Figure 4. Selected FT-IR spectra recorded at various temperatures for compound $(\text{mimC}_{18})_{37}\{\text{Mo}_{132}\}$ under nitrogen.

2.2. Liquid Crystal Properties

2.2.1. Polarized Optical Microscopy

The liquid crystal properties of all the compounds were examined by temperature dependent polarized optical microscopy (TD-POM) between two glass plates. Under heating our materials from room temperature to their decomposition temperatures, the TD-POM revealed the formation of relatively fluid birefringent and homogenous textures characteristic of the liquid crystalline nature for the samples $(\text{mimC}_{12})_{36}\text{-Mo}_{132}$, $(\text{mimC}_{14})_{38}\text{-Mo}_{132}$, $(\text{mimC}_{16})_{41}\text{-Mo}_{132}$, $(\text{mimC}_{18})_{37}\text{-Mo}_{132}$, and $(\text{mimC}_{20})_{37}\text{-Mo}_{132}$ in the 100–240 °C temperature range as shown in Figure 5. Furthermore, the samples did not show characteristic textures due to their decomposition before reaching the isotropic state and consequently it is difficult to identify the type of the mesophase from the TD-POM pictures. However, the three mixed compounds, $(\text{mimC}_{12})_{20}(\text{mimC}_{20})_{20}\text{-Mo}_{132}$, $(\text{mimC}_{12})_{33}(\text{mimC}_{20})_{7}\text{-Mo}_{132}$ and $(\text{mimC}_{12})_{8}(\text{mimC}_{20})_{33}\text{-Mo}_{132}$ do not show birefringent textures, even at high temperature, indicating the lack of liquid crystal properties for these compounds.

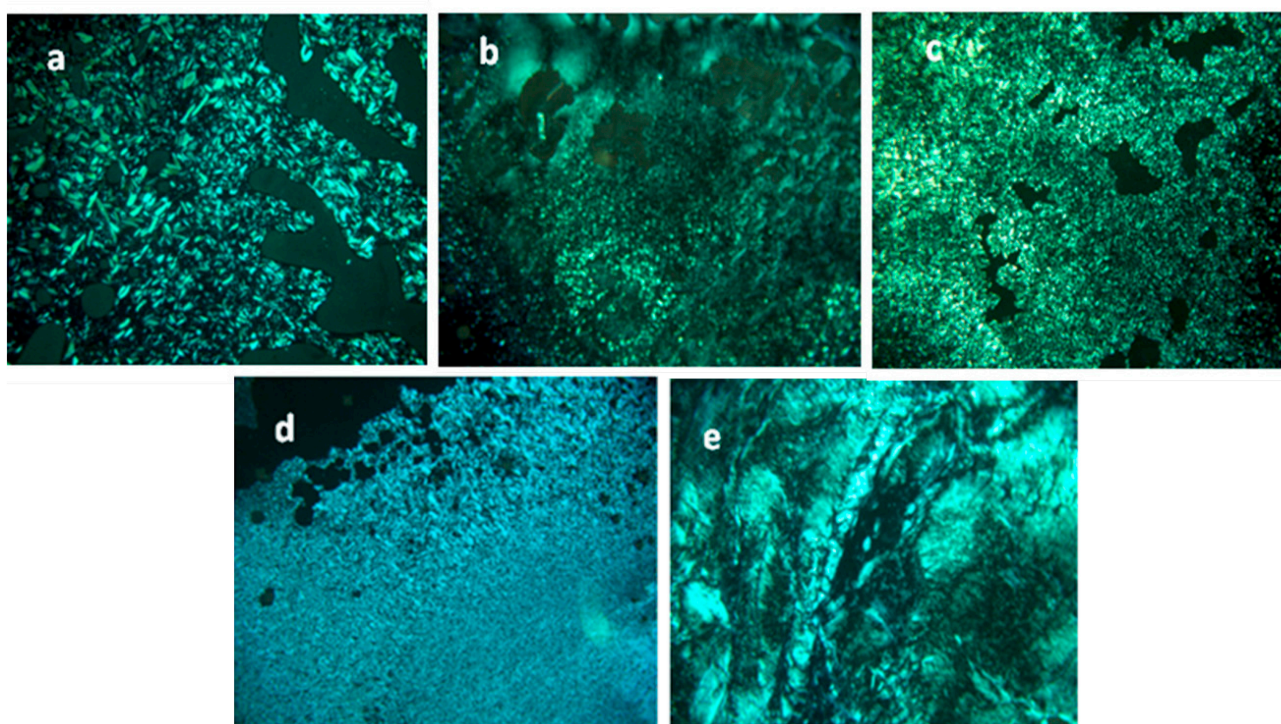


Figure 5. Polarized Optical Microphotographs of $(\text{mimC}_{12})_{36}\text{-Mo}_{132}$ at 113 °C (a), $(\text{mimC}_{14})_{38}\text{-Mo}_{132}$ at 220 °C (b), $(\text{mimC}_{16})_{41}\text{-Mo}_{132}$ at 160 °C (c), $(\text{mimC}_{18})_{37}\text{-Mo}_{132}$ at 100 °C (d), and $(\text{mimC}_{20})_{37}\text{-Mo}_{132}$ at 200 °C (e).

2.2.2. Differential Scanning Calorimetry

The DSC curves of the Keplerate-based materials were recorded under nitrogen at a scan rate of 5 °C/min between –40 °C and 220–260 °C. At least three thermal cycles were achieved and the obtained results for the second thermal cycles are shown in Figure 6, while the thermodynamic parameters are listed in Table 2.

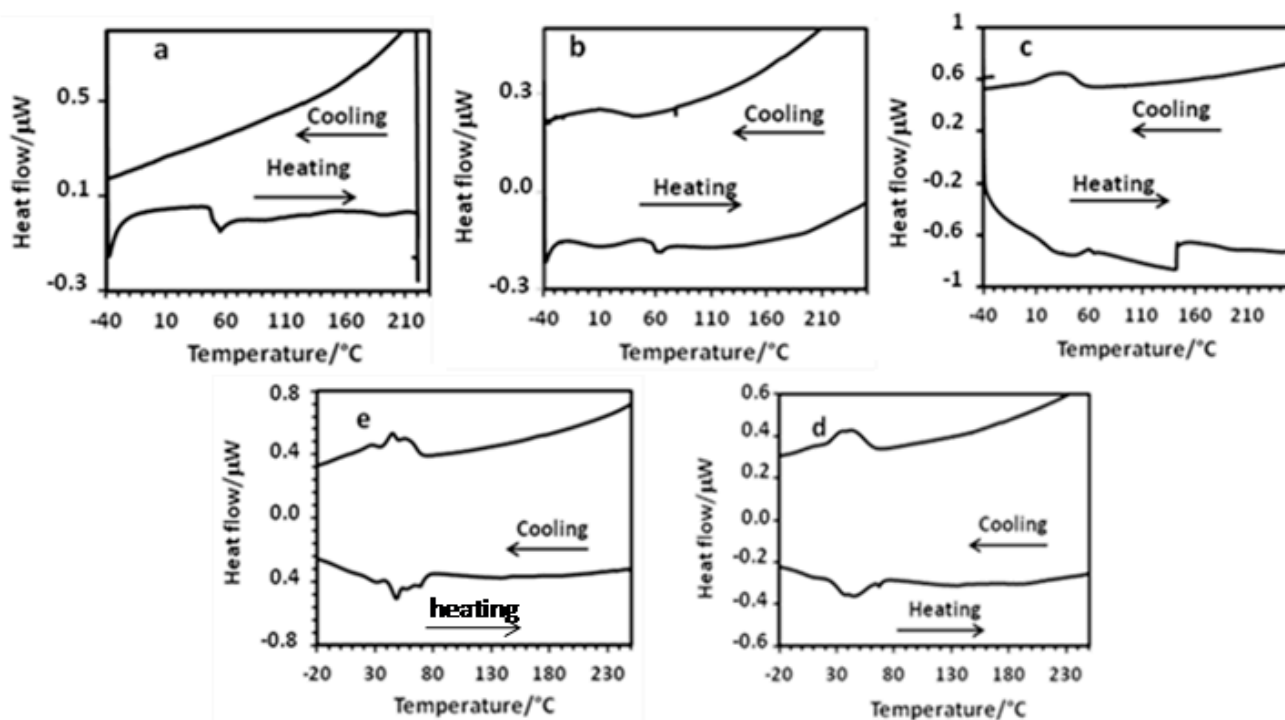


Figure 6. DSC traces of the second thermal cycle recorded under N₂ (5 °C min⁻¹) for (mimC₁₂)₃₆-Mo₁₃₂ (a), (mimC₁₄)₃₈-Mo₁₃₂ (b), (mimC₁₆)₄₁-Mo₁₃₂ (c), (mimC₁₈)₃₇-Mo₁₃₂ (d), (mimC₂₀)₃₇-Mo₁₃₂ (e).

Table 2. Temperatures, melting enthalpy and entropy changes of the phase transitions between the glassy state and the liquid crystal phases observed for the materials exhibiting liquid crystalline properties. Temperatures are given for the peaks observed by DSC measurements during the second heating process.

Compounds	<i>T</i> /°C (Heating Mode)	<i>MM</i> g/mol	<i>n</i> (CH ₂)	ΔH_m /kJ·mol ⁻¹	ΔS_m /J·mol ⁻¹ ·K ⁻¹	$\Delta H'_m$ ^a /J·mol ⁻¹	$\Delta S'_m$ ^a /J·mol ⁻¹ ·K ⁻¹
(mimC ₁₂) ₃₆ -Mo ₁₃₂	+55	30982	396	-4.3	-13	-10.95	-0.03
(mimC ₁₄) ₃₈ -Mo ₁₃₂	+13	32387	494	-46.3	-162	-94	-0.33
(mimC ₁₆) ₄₁ -Mo ₁₃₂	+31	34889	615	-204.1	-671	-331.8	-1.1
(mimC ₁₈) ₃₇ -Mo ₁₃₂	+43	35059	629	-158.5	-501	-252	-0.8
(mimC ₂₀) ₃₇ -Mo ₁₃₂	+46	36006	703	-163.8	-514	-233	0.73
DODA ₃₆ -Mo ₁₃₂ [37]	+9	42982	1224	-849.0	-3009	-639	-2.45
DODA ₄₄ -Mo ₁₃₂ S ₆₀ [36]	+9	47838	1548	-1333.0	-4724	-918	-3.25
DODA ₅₆ -Mo ₁₃₂ S ₆₀ [36]	+9	55357	1904	-1649.0	-5848	-866	-3.07
DODACl	+18	586.5	34	-83.1	-278.5	-2445	-8.19

^a $\Delta Y'_m = \Delta Y_m/n(\text{CH}_2)$ (*Y* = H, S) where *n*(CH₂) corresponds to the total number of methylene groups of the alkyl chains borne by the cations.

Globally, the DSC curves exhibit very broad and often composite first-order phase transitions for the melting of the solid to give the mesophase. This contrasts with the relatively sharp first-order phase transitions reported for DODA⁺ salts of Keplerate Mo₁₃₂ and Mo₁₃₂S₆₀ [36,37]. These results suggest that the local molecular or supramolecular mobility is insufficient to allow the development of a network of intermolecular interactions sufficiently regular to obtain a well-developed mesophase. In

addition, excepted for $(\text{mimC}_{12})_{36}\text{-Mo}_{132}$, the melting transitions appear reversible for the other compounds even if it can be broader for some compounds such as $(\text{mimC}_{14})_{38}\text{-Mo}_{132}$ for example.

The average melting transition temperatures, which are determined in the heating mode, are summarized in Table 2. In short, disregarding the compound $(\text{mimC}_{12})_{36}\text{-Mo}_{132}$, the melting transition temperatures increase roughly linearly in the series $(\text{mimC}_{14})_{38}\text{-Mo}_{132}$, $(\text{mimC}_{16})_{41}\text{-Mo}_{132}$, $(\text{mimC}_{18})_{37}\text{-Mo}_{132}$, and $(\text{mimC}_{20})_{37}\text{-Mo}_{132}$ from +13 °C to +46 °C, when the alkyl chain length of the imidazolium cation increases, and are significantly different from those obtained with the three previous DODA⁺ salts (+9 °C) [36,37].

The corresponding melting enthalpy and entropy changes, ΔH_m and ΔS_m , are also gathered in Table 2. A comparison of these values remains difficult since the number of cations can vary in the series of Mo_{132} -based materials. The weighted $\Delta H'_m$ and $\Delta S'_m$ values correspond to the ratios $\Delta H_m/n(\text{CH}_2)$ and $\Delta S_m/n(\text{CH}_2)$ respectively, where $n(\text{CH}_2)$ is the total number of methylene groups in the compounds, and is more convenient. The plot of $-\Delta H'_m$ versus $-\Delta S'_m$ including data previously reported for DODA salts and DODACl alone is given in Figure 7. It displays a linear relationship typical for H/S compensation [40] and evidences two sets of points : one corresponding to the imidazolium salts of Mo_{132} of this study, $(\text{mimC}_{14})_{38}\text{-Mo}_{132}$, $(\text{mimC}_{16})_{41}\text{-Mo}_{132}$, $(\text{mimC}_{18})_{37}\text{-Mo}_{132}$, and $(\text{mimC}_{20})_{37}\text{-Mo}_{132}$ and one corresponding to the DODA⁺ salts $(\text{DODA})_{36}\text{-Mo}_{132}$, $(\text{DODA})_{44}\text{-Mo}_{132}\text{S}_{60}$, $(\text{DODA})_{56}\text{-Mo}_{132}\text{S}_{60}$ bearing liquid crystalline properties [36,37], whereas DODACl appears clearly different. For DODACl, the alkyl chains are weakly constrained by the presence of the counter chloride anion and the melting of the chains follows the trend expected for simple alkanes [40]. Figure 7 suggests that the alkyl chains of the cations associated to Mo_{132} are strongly perturbed by the presence of the Keplerate capsule. From a macroscopic point of view, it results in a drastic lowering of the fluidity of the samples. This phenomenon is more pronounced for the series of imidazolium salts than for the three DODA⁺ salts. Furthermore, as seen in the insert of the Figure 7, the ratio $\Delta H'_m/\Delta S'_m$ appears globally correlated for the series of imidazolium salts of Mo_{132} . The magnitude of the $\Delta H_m/n\text{CH}_2$ and $\Delta S_m/n\text{CH}_2$ ratios seems to be strongly and linearly correlated with the average closeness of the $-\text{CH}_2-$ with the surface of the anions. In other words, the $-\text{CH}_2-$ located closer to the surface are more constrained than those which are more distant. It is as if the $-\text{CH}_2-$ located in a crown close to the surface were “frozen” and consequently no more available for melting. This may explain why the fluidity of the samples bearing long aliphatic chains is higher.

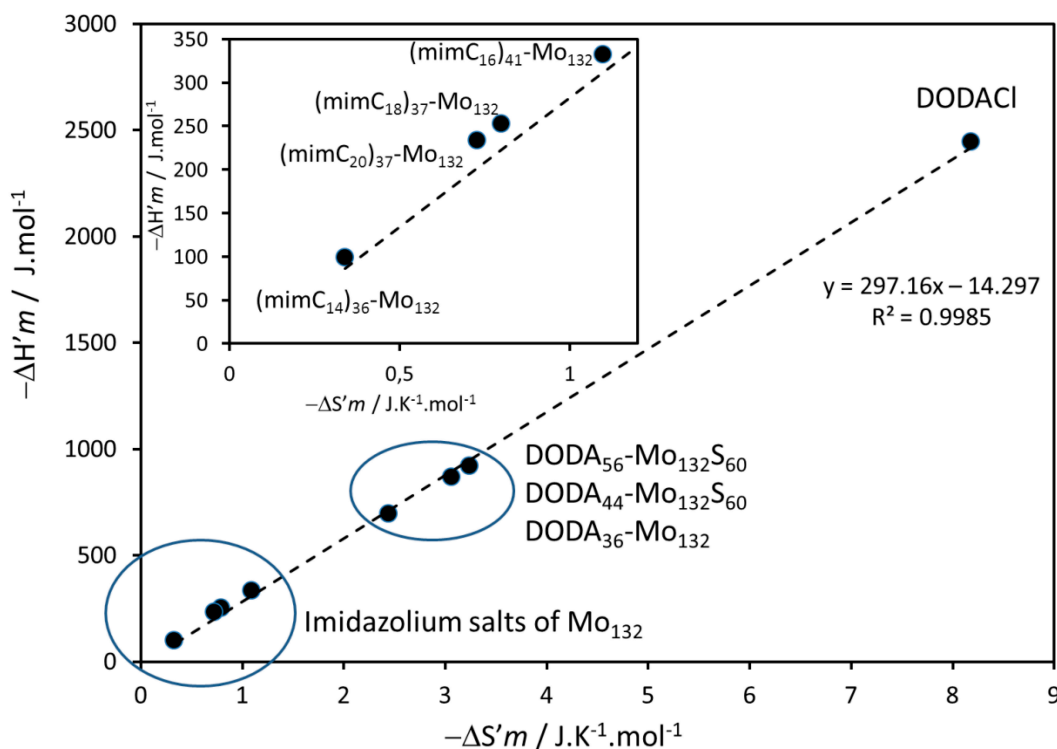


Figure 7. $\Delta H'_m$ versus $\Delta S'_m$ plot.

2.2.3. Small-Angle X-ray Diffraction Studies

Small-angle X-ray Diffraction (SA-XRD) experiments (from -40 to 200 °C temperature range) were carried out to elucidate the nature of the liquid crystalline phases. Arbitrarily, we have chosen to present the SA-XRD patterns obtained at 200 °C, when possible, for two main reasons: (i) to compare with the previous data published at the same temperature [36,37], (ii) at this temperature the fluidity is relatively high and results in sharper peaks. The resulting SA-XRD patterns are depicted in Figure 8, whereas the corresponding data are summarized in Table 3.

Globally, in contrast with the previous DODA⁺ salts, which exhibited up to three sharp equidistant reflections indexed as the 001, 002 and 003 Miller indices in addition to a broad and diffuse signal at approximately 4.5 Å associated with the liquid-like molten chains of the DODA⁺, the imidazolium salts display broader reflections with no signal which can be attributed to the molten chains.

The three compounds **(mimC₁₄)₃₈-Mo₁₃₂**, **(mimC₁₈)₃₇-Mo₁₃₂** and **(mimC₂₀)₃₇-Mo₁₃₂** unambiguously display two lines indexed as 001 and 002 reflections which are characteristic of a 1D lamellar ordering, whereas the two compounds **(mimC₁₂)₃₆-Mo₁₃₂** and **(mimC₁₆)₄₁-Mo₁₃₂** exhibits three broad lines for which we were not able to give a realistic indexation. Interestingly, the three mixed compounds **(mimC₁₂)₂₀(mimC₂₀)₂₀-Mo₁₃₂**, **(mimC₁₂)₃₃(mimC₂₀)₇-Mo₁₃₂** and **(mimC₁₂)₈(mimC₂₀)₃₃-Mo₁₃₂** also display the 001 and 002 lines, whereas no liquid crystals behaviors and no first-order phase transition were detected by TD-POM and DSC, respectively. For the two latter mixed salts, we also noticed that increasing temperature above 160 – 180 °C produces unidentified additional reflections, which suggests either a degradation of the product or the existence of a mixture of different compounds in the solid.

The results obtained for the mixed salts demonstrate the propensity for this family of salts to self-organize in a lamellar fashion even in the solid state.

Focusing on the major part of our materials, a 1D lamellar ordering is evidenced and the interlayer spacing h can be deduced since it corresponds to the d_{001} distance. These values are listed in Table 3 and are found in the range 31.34 to 35.57 Å, in agreement with the values found for the DODA⁺ salts (DODA)₃₆-Mo₁₃₂, (DODA)₄₄-Mo₁₃₂S₆₀ and (DODA)₅₆-Mo₁₃₂S₆₀ for which h was found between 26.90 Å and 34.55 Å [36,37]. As mentioned previously, such a lamellar organization could appear surprising if we consider the spherical shape of the cluster. Nevertheless, previous studies clearly confirm the capability of Mo₁₃₂ to assemble into lamellar aggregates [34,36,37].

Regarding the ionic character of these materials, the positive charges the imidazolium cations are necessarily located close to the spherical surface of the keplerate Mo₁₃₂. Logically, taking into account the isotropic shape of the Keplerate, imidazolium or DODA⁺ cations should be randomly distributed onto the surface. Interestingly, the situation can be very different in the solid or the liquid crystalline states. In particular, if a deformation is required to minimize the electric multipolar interactions, the system can be distorted. When the starting object is a sphere, an elongation or a compression may occur, thus leading to the formation of ellipsoids, which are compatible with lamellar organizations. As the central Mo₁₃₂ core is rigid, the deformation can only come from the non-uniform distribution of the cations around the spherical Keplerate [37].

In all cases, the diameter of the anionic inorganic cores (≈ 30 Å) is of the same order of the lamellar periodicity h (31.34 to 35.57 Å range), which implies that the layers of the lamellar phases are composed of oblate clusters where cations are globally distributed in a plan around the Mo₁₃₂ sphere corresponding to the plans of the sheets. Taking into account a realistic density of $d = 1.0$ g cm⁻³ in the mesophase [36,37,41] and assuming that clusters are locally ordered in a compact hexagonal lattice with one cluster per unit cell ($Z = 1$) [36,37], we can thus calculate the hexagonal lattice parameter a_{hex} by using Equation (1), where MM_C is the molar mass of the cluster, h the interlayer spacing, d the density and N_{AV} , the Avogadro number.

$$a_{\text{Hex}} = \left(\frac{2 \cdot Z \cdot MM_C}{h \cdot d \cdot N_{\text{AV}} \cdot 10^{-24} \cdot 3^{1/2}} \right)^{1/2} \quad (1)$$

We calculate $41.79 \leq a_{\text{hex}} \leq 45.29$ Å, which are smaller than the parameters found for DODA salts [36,37], but in good agreement with $a_{\text{hex}} = 45$ Å reported by Volkmer and Müller [34] for a hexagonal monolayer of (DODA)₃₆-Mo₁₃₂.

Considering the fixed size of the inorganic cluster (≈ 30 Å) and the size of cations in a linear configuration ranging from 20 Å for mimC₁₂⁺ to 30 Å for mimC₂₀⁺, the a_{hex} distances which correspond to the distance between two clusters within the layers implies some folding of the alkyl chains of the cations. Indeed, the hypothesis of linear arrangements of the alkyl chains of the imidazolium cations accompanied by full interdigitation of the alkyl chains with the neighboring clusters would lead to a_{hex} distances of at least 50–55 Å as found for the DODA⁺ salts ($51.54 \leq a_{\text{hex}} \leq 55.21$ Å). In contrast to the DODA⁺ cations, in which the two neighboring octadecyl chains favor the organization of the cations through van der Waals interactions, the alkyl chains of the imidazolium cations are

probably folded, prohibiting the interdigitation with the neighboring cations, a situation not favorable for the development of well-ordered mesophases.

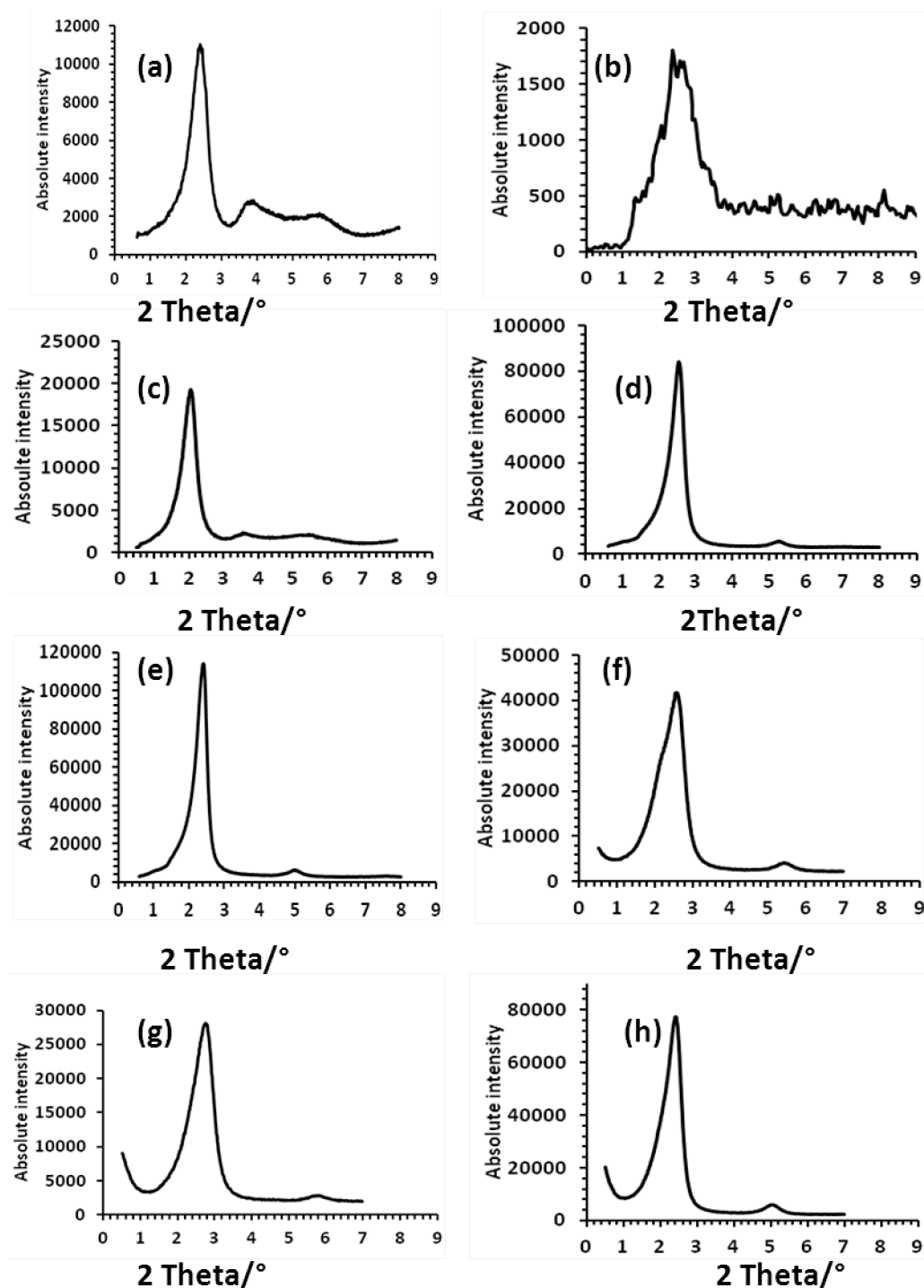


Figure 8. SA-XRD patterns recorded at 200 °C for **(mimC₁₂)₃₆-Mo₁₃₂** (a), **(mimC₁₄)₃₈-Mo₁₃₂** (b), **(mimC₁₆)₄₁-Mo₁₃₂** (c), **(mimC₁₈)₃₇-Mo₁₃₂** (d), **(mimC₂₀)₃₇-Mo₁₃₂** (e), **(mimC₁₂)₂₀(mimC₂₀)₂₀-Mo₁₃₂** (f), **(mimC₁₂)₃₃(mimC₂₀)₇-Mo₁₃₂** at 140 °C (g), **(mimC₁₂)₈(mimC₂₀)₃₃-Mo₁₃₂** (h).

Table 3. Indexation at 200 °C during the cooling mode for the reflections detected in the liquid-crystalline phase by SA-XRD.

Compounds	d_{hkl} Measured/Å	<i>I</i> /a.u.	Indexation	Cell Parameters/Å
(mimC ₁₂) ₃₆ -Mo ₁₃₂	36.90	VS	c	
	23.19	MW (broad)	c	
	15.45	MW (broad)	c	
(mimC ₁₄) ₃₈ -Mo ₁₃₂ ^a	35.57	S	001	$h = 35.57$ $a_{\text{hex}} = 41.79$
(mimC ₁₆) ₄₁ -Mo ₁₃₂	40.71	VS	c	
	24.55	MW (broad)	c	
	16.52	MW (broad)	c	
(mimC ₁₈) ₃₇ -Mo ₁₃₂	32.78	VS	001	$h = 32.78$
	16.34	W	002	$a_{\text{hex}} = 45.29$
(mimC ₂₀) ₃₇ -Mo ₁₃₂	35.34	VS	001	$h = 35.34$
	17.67	W	002	$a_{\text{hex}} = 44.21$
(mimC ₁₂) ₂₀ (mimC ₂₀) ₂₀ -Mo ₁₃₂	32.91	VS	001	$h = 32.91$
	16.26	W	002	$a_{\text{hex}} = 44.98$
(mimC ₁₂) ₃₃ (mimC ₂₀) ₇ -Mo ₁₃₂ ^b	31.34	VS	001	$h = 31.34$
	15.22	W	002	$a_{\text{hex}} = 45.23$
(mimC ₁₂) ₈ (mimC ₂₀) ₃₃ -Mo ₁₃₂	35.30	VS	001	$h = 35.30$
	17.60	W	002	$a_{\text{hex}} = 43.42$
DODA ₃₆ {Mo ₁₃₂ } [37]	26.9	VS	001	$h = 26.9$
	13.3	M	002	$a_{\text{hex}} = 54.2$
	9.1	W	003	
DODA ₄₄ {Mo ₁₃₂ S ₆₀ } [36]	34.20	VS	001	$h = 34.12$
	16.98	M	002	$a_{\text{hex}} = 51.64$
	11.40	W	003	
DODA ₅₆ {Mo ₁₃₂ S ₆₀ } [36]	34.91	VS	001	$h = 34.55$
	17.09	M	002	$a_{\text{hex}} = 55.21$

^a measured at 190 °C; ^b measured at 140 °C; ^c not determined. *I* corresponds to the intensity of the reflections (VS: very strong, S: strong, M: medium, W: weak, VW: very weak); *h* is the lattice parameter of the lamellar phase; a_{hex} is the local hexagonal organization within the layers calculated with Equation 1.

3. Experimental Section

3.1. Fourier Transformed Infrared (FT-IR) Spectra

Fourier Transformed Infrared (FT-IR) spectra were recorded on a 6700 FT-IR Nicolet spectrophotometer (Les Ulis, France), using diamond ATR technique. The spectra were recorded on undiluted samples and ATR correction was applied. The variable temperature FT-IR spectra were recorded on an IRTF Nicolet iS10 spectrometer (Les Ulis, France) in diffuse reflectance mode by using high temperature diffuse reflectance environmental chamber. The background was recorded using dry KBr at 150 °C and the samples were diluted into a KBr matrix (about 10% of compound)

before heating. The FT-IR spectra were recorded in the 20–500 °C temperature range under air or under nitrogen with a heating rate of 2 °C min⁻¹.

3.2. Elemental Analyses

Elemental analyses were performed by the service central d'analyses du CNRS, Vernaison, France and by the service d'analyses du CNRS, ICSN, Gif sur Yvette, France.

3.3. Water Content

Water content was determined by thermal gravimetric (TGA) analysis with a Seiko TG/DTA 320 thermogravimetric balance (5 °C min⁻¹, under air) (Chiba, Japan).

3.4. Nuclear Magnetic Resonance (NMR)

Solution ¹H NMR measurements were performed on a Bruker Avance 300 instrument (Wissembourg, France) operating at 300 MHz in 5 mm o.d. tubes. Chemical shifts were referenced to TMS.

3.5. Differential Scanning Calorimetry (DSC)

DSC traces were obtained with a Mettler Toledo DSC1 Star Systems differential scanning calorimeter (Greifensee, Switzerland) from 3 to 5 mg samples (5 °C min⁻¹, under N₂). Several thermal cycles were performed between 40 °C and 220 °C, the first one allowing the removal of water and the organization of the solid, the following cycles explored the reproducibility and the thermal stability of the materials in this temperature range.

3.6. Temperature Dependent Polarized Optical Microscopy (TD-POM)

Temperature dependent polarized optical microscopy (TD-POM) characterizations of the optical textures of the mesophases were performed with a Leitz Orthoplan Pol polarizing microscope (Brugg, Switzerland) with a Leitz LL 20°/0.40 polarizing objective and equipped with a Linkam THMS 600 variable temperature stage (Brugg, Switzerland).

3.7. Small Angle X-ray Diffraction (SA-XRD)

The crude powder was filled in Lindemann capillaries of 0.8 mm diameter. For almost all our materials, the diffraction patterns were performed on an Empyrean (PANalytical) diffractometer (Zurich, Switzerland) in capillary mode, with a focusing X-ray mirror for Cu radiation and a PIXcel3D area detector. For the compound **(mimC₁₄)₃₆-Mo₁₃₂** experiments were performed with a STOE transmission powder diffractometer system STADI P (Darmstadt, Germany) using a focused monochromatic Cu-K_{α1} beam obtained from a curved Germanium monochromator (Johann-type, STOE, Darmstadt, Germany) and collected on a curved image plate position-sensitive detector (IP-PSD). A calibration with silicon and copper laurate standards, for high and low angle domains, respectively, was preliminarily performed. Sample capillaries were placed in the high-temperature

furnace for measurements in the range of desired temperatures (from -40 up to 240 °C) within 0.05 °C. Periodicities up to 50 Å could be measured. The exposure times were of 15 min.

3.8. Synthesis of Mo_{132} -Based Materials

The precursor compound $(NH_4)_{42}[Mo_{132}O_{372}(CH_3COO)_{30}(H_2O)_{72}] \cdot 300H_2O \cdot ca.10CH_3COONH_4$ noted NH_4-Mo_{132} was prepared as described by Müller *et al.* [42]. 1-methyl-3-alkylimidazolium bromides salts were prepared as described previously and characterized by routine 1H NMR in $CDCl_3$ [38].

3.9. General Preparation of Mo_{132} -Based Materials

The Keplerate-based materials were prepared as follows: NH_4-Mo_{132} (300 mg, 0.01 mmol) was dissolved in 30 mL of water and then a chloroform solution containing the organic cations (≈ 168 equivalents / NH_4-Mo_{132} , 1.72 mmol). The mixture was stirred for 1 h, where the Keplerate was totally transferred into the organic phase as indicated by the colorless aqueous phase. The organic phase was then separated and the target materials were precipitated from the organic phase by addition of an excess of ethanol, isolated by filtration, washed with ethanol, dried in air and characterized by FT-IR, EDX, Elemental Analyses, TGA and 1H NMR.

3.9.1. $(mimC_{12}H_{25})_{36}(NH_4)_4[Mo_{132}O_{372}(CH_3COO)_{30}(H_2O)_{72}] \cdot 38H_2O$, $(mimC_{12})_{36}-Mo_{132}$

It was prepared using $mimC_{12}Br$ (582 mg, 1.76 mmol). Yield 200 mg, 63%. IR/ cm^{-1} : 2922 (vs), 2852 (s), 1553 (s), 1442 (m), 1163 (m), 975 (vs), 940 (s), 855(s) 801 (vs), 727 (s), 635 (m), 573 (s). Elemental analysis calcd. (%) for $(mimC_{12}H_{25})_{36}(NH_4)_6[Mo_{132}O_{372}(CH_3COO)_{30}(H_2O)_{72}] \cdot 38H_2O$ ($M = 31529$ g·mol $^{-1}$) C 24.23; H, 4.64; N, 3.47; Mo, 40.17. Found C, 24.30; H, 4.45; N, 3.39; Mo, 39.28. EDX only evidenced Mo and shows no traces of Br which could be due to an excess of the starting salt. Thermogravimetric analysis (TGA) suggests a mass loss of 6% from room temperature to 188 °C corresponding to crystallization and coordinated water molecules (calcd.: 6.3%).

3.9.2. $(mimC_{14}H_{29})_{38}(NH_4)_4[Mo_{132}O_{372}(CH_3COO)_{30}(H_2O)_{72}] \cdot 30H_2O$, $(mimC_{14})_{38}-Mo_{132}$

It was prepared using $mimC_{14}Br$ (634 mg, 1.76 mmol). Yield 269 mg, 80%. IR/ cm^{-1} : 2920 (m), 2850 (m), 1547 (m), 1440 (m), 1161 (m), 974 (vs), 939 (s), 789 (vs), 711 (vs), 563 (vs), 410 (vs). Elemental analysis calcd. (%) for $(mimC_{14}H_{29})_{38}(NH_4)_4[Mo_{132}O_{372}(CH_3COO)_{30}(H_2O)_{72}] \cdot 30H_2O$ ($M = 32461$ g·mol $^{-1}$) C 26.12; H, 5.09; N, 3.45; Mo, 39.01. Found C, 26.22; H, 4.90; N, 3.30; Mo, 39.28. EDX only evidenced Mo and shows no traces of Br which could be due to an excess of the starting salt. Thermogravimetric analysis (TGA) suggests a mass loss of 5.4% from room temperature to 135 °C corresponding to crystallization and coordinated water molecules (calcd.: 5.6%).

3.9.3. $(mimC_{16}H_{33})_{41}(NH_4)_1[Mo_{132}O_{372}(CH_3COO)_{30}(H_2O)_{72}] \cdot 38H_2O$, $(mimC_{16})_{41}-Mo_{132}$

It was prepared using $mimC_{16}Br$ (683 mg, 1.76 mmol). Yield 350 mg, quantitative yield. IR/ cm^{-1} : 3451 (m), 2923 (s), 2853 (m), 1560 (m), 1466 (m), 1164 (m), 976 (vs), 941 (m), 807 (vs), 729 (vs), 577 (s), 415 (vs). Elemental analysis calcd. (%) for $(mimC_{16}H_{33})_{41}(NH_4)_3[Mo_{132}O_{372}(CH_3COO)_{30}(H_2O)_{72}] \cdot 48H_2O$ ($M = 34889.2$ g·mol $^{-1}$) C 29.61; H, 5.62; N, 3.25; Mo, 36.33. Found C, 29.60; H, 5.48; N, 3.39;

Mo, 36.3. EDX only evidenced Mo and shows no traces of Br which could be due to an excess of the starting salt. Thermogravimetric analysis (TGA) suggests a mass loss of 6.4% from room temperature to 150 °C corresponding to crystallization and coordinated water molecules (calcd.: 6.2%).

3.9.4. (mimC₁₈H₃₇)₃₇(NH₄)₅[Mo₁₃₂O₃₇₂(CH₃COO)₃₀(H₂O)₇₂] \cdot 48H₂O, (mimC₁₈)₃₇-Mo₁₃₂

It was prepared using mimC₁₈Br (732 mg, 1.76 mmol). Yield 355 mg, 96%. IR/cm⁻¹: 2919 (s), 2849 (m), 1555 (m), 1424 (m), 1161 (m), 975 (s), 941 (s), 854 (s), 791 (vs), 713 (vs), 565 (vs), 411 (vs). Elemental analysis calcd. (%) for (mimC₁₈H₂₉)₄₀(NH₄)₃[Mo₁₃₂O₃₇₂(CH₃COO)₃₀(H₂O)₇₂] \cdot 48H₂O (M = 35058.68 g \cdot mol⁻¹) C 29.88; H, 5.57; N, 3.11; Mo, 36.28 Found C, 29.94; H, 5.58; N, 3.15; Mo, 36.13. EDX only evidenced Mo and shows no traces of Br which could be due to an excess of the starting salt. Thermogravimetric analysis (TGA) suggests a mass loss of 6.25% from room temperature to 188 °C corresponding to crystallization and coordinated water molecules (calcd.: 6.16%).

3.9.5. (mimC₂₀H₄₁)₃₇(NH₄)₅[Mo₁₃₂O₃₇₂(CH₃COO)₃₀(H₂O)₇₂] \cdot 43H₂O, (mimC₂₀)₃₇-Mo₁₃₂

It was prepared using mimC₂₀Br (780 mg, 1.76 mmol). Yield 0.35 mg, 92%. IR/cm⁻¹: 2919 (s), 2850 (s), 1541 (m), 1443 (m), 1162 (m), 973 (s), 938 (s), 854 (s), 792 (vs), 632 (vs), 565 (vs), 411 (vs). Elemental analysis calcd. (%) for (mimC₂₀H₄₁)₃₇(NH₄)₅[Mo₁₃₂O₃₇₂(CH₃COO)₃₀(H₂O)₇₂] \cdot 43H₂O (M = 36006.57 g \cdot mol⁻¹) C 31.62; H, 5.81; N, 3.07; Mo, 35.17. Found C, 31.36; H, 5.51; N, 3.07; Mo, 35.12. EDX only evidenced Mo and shows no traces of Br which could be due to an excess of the starting salt. Thermogravimetric analysis (TGA) suggests a mass loss of 5.5% from room temperature to 160 °C corresponding to crystallization and coordinated water molecules (calcd.: 5.7%).

3.9.6. (mimC₁₂H₂₅)₂₀(mimC₂₀H₃₃)₂₀(NH₄)₂[Mo₁₃₂O₃₇₂(CH₃COO)₃₀(H₂O)₇₂] \cdot 38H₂O, (mimC₁₂)₂₀(mimC₂₀)₂₀-Mo₁₃₂

It was prepared using mimC₂₀Br (390 mg, 0.882 mmol) and mimC₁₂Br (290 mg, 0.882 mmol). Yield 100 mg, 28%. IR/cm⁻¹: 2920 (vs), 2849 (s), 1557 (m), 1442 (m), 1162 (m), 972 (vs), 940 (s), 854 (s), 798 (vs), 570 (s), 412 (s). Elemental analysis calcd. (%) for (mimC₁₂H₂₅)₂₀(mimC₂₀H₃₃)₂₀(NH₄)₂[Mo₁₃₂O₃₇₂(CH₃COO)₃₀(H₂O)₇₂] \cdot 38H₂O (M = 34709.05 g \cdot mol⁻¹) C 29.75; H, 5.45; N, 3.30. Found C, 29.70; H, 5.63; N, 3.25. EDX atomic ratios calculated for (mimC₁₂)₂₀(mimC₂₀)₂₀-{Mo₁₃₂} shows no Br or traces. Thermogravimetric analysis (TGA) suggests a mass loss of 5.7% from room temperature to 170 °C corresponding to crystallization and coordinated water molecules (calcd.: 5.7%) and % org: 42.5% (calcd. 40.6%).

3.9.7. (mimC₁₂H₂₅)₃₃(mimC₂₀H₃₃)₇(NH₄)₂[Mo₁₃₂O₃₇₂(CH₃COO)₃₀(H₂O)₇₂] \cdot 48H₂O, (mimC₁₂)₃₃(mimC₂₀)₇-Mo₁₃₂

It was prepared using mimC₁₂Br (462 mg, 1.41 mmol) and mimC₂₀Br (156 mg, 0.34 mmol). Yield 120 mg, 34.3%. IR/cm⁻¹. 2922 (vs), 2851 (s), 1557 (s), 1444 (m), 1163 (m), 973 (vs), 941 (s), 855 (s), 799 (s), 724 (vs), 570 (vs), 412 (vs). Elemental analysis calcd. (%) for (mimC₁₂H₂₅)₃₃(mimC₂₀H₃₃)₇(NH₄)₂[Mo₁₃₂O₃₇₂(CH₃COO)₃₀(H₂O)₇₂] \cdot 38H₂O (M = 33430.45 g \cdot mol⁻¹) C 27.16; H, 5.09; N, 3.43. Found C, 27.30; H, 5.01; N, 3.14. EDX only evidenced Mo and shows no

traces of Br which could be due to an excess of the starting salt. Thermogravimetric analysis (TGA) suggests a mass loss of 6.6% from room temperature to 170 °C corresponding to crystallization and coordinated water molecules (calcd.: 6.4%) and % org: 37.4 (calcd. 37.4%).

3.9.8. $(\text{mimC}_{12}\text{H}_{25})_8(\text{mimC}_{20}\text{H}_{33})_{33}(\text{NH}_4)_1[\text{Mo}_{132}\text{O}_{372}(\text{CH}_3\text{COO})_{30}(\text{H}_2\text{O})_{72}] \cdot 38\text{H}_2\text{O}$,
 $(\text{mimC}_{12})_8(\text{mimC}_{20})_{33}-\text{Mo}_{132}$

It was prepared using $\text{mimC}_{12}\text{Br}$ (120 mg, 0.35 mmol) and $\text{mimC}_{20}\text{Br}$ (620 mg, 1.4 mmol). Yield 110 mg, 30.5%. IR/cm⁻¹: 2923 (vs), 2852 (s), 1559 (s), 1465 (m), 1163 (s), 976 (vs), 941 (vs), 859 (vs), 732 (vs), 576 (s), 412 (vs). Elemental analysis calcd. (%) for $(\text{mimC}_{12}\text{H}_{25})_8(\text{mimC}_{20}\text{H}_{33})_{33}(\text{NH}_4)_2[\text{Mo}_{132}\text{O}_{372}(\text{CH}_3\text{COO})_{30}(\text{H}_2\text{O})_{72}] \cdot 38\text{H}_2\text{O}$ (M = 34709.05 g·mol⁻¹) C 32.17; H, 5.87; N, 3.17. Found C, 32.11; H, 5.71; N, 3.24. EDX atomic ratios calculated for $(\text{mimC}_{12})(\text{mimC}_{20})-\{\text{Mo}_{132}\}$ shows no Br or traces. Thermogravimetric analysis (TGA) suggests a mass loss of 5.7% from room temperature to 170 °C corresponding to crystallization and coordinated water molecules (calcd.: 5.7%) and org: 46.8% (calcd. 49%).

4. Conclusions

In the following of our previous works describing the liquid crystal properties of Keplerates associated to DODA⁺ cations or of the nanoscopic inorganic cluster $[\text{K}_2\text{Na}_x\text{Li}_y\text{H}_z\{\text{Mo}_4\text{O}_4\text{S}_4(\text{OH})_2 \cdot (\text{H}_2\text{O})_3\}_2(\text{P}_8\text{W}_{48}\text{O}_{184})]^{(34-x-y-z)-}$ combined with alkylmethylimidazolium cations, we prepared in this study a series of eight new compounds resulting from the ionic association of the nanoscopic inorganic cluster $[\text{Mo}_{132}\text{O}_{372}(\text{CH}_3\text{COO})_{30}(\text{H}_2\text{O})_{72}]^{42-}$ with various alkylmethylimidazolium cations, denoted mimC_n^+ ($n = 12-20$). The results obtained in this study confirm that the strategy which consists in associating highly charged polyoxometalate clusters with very simple organic cations bearing only alkyl chains of variable sizes can provide liquid crystalline phases. The latter were investigated by TD-POM, DSC and SA-XRD. The major part of the synthesized materials exhibit lamellar organization in the solid state or in the liquid crystalline phase. However, DSC shows very broad phase transitions between the solid and the mesophase which could be explained by insufficient supramolecular mobility to develop network of intermolecular interactions. The small angle-X ray diffraction studies provide the interlayer spacing h and the hexagonal lattice parameter a_{hex} , which evidence a non-uniform distribution of the imidazolium cations around the spherical clusters **Mo**₁₃₂ and a folding of the alkyl chains. This lead to less interdigitation between the alkyl chains of the cations and therefore to poorly organized mesophases. This observation contrasts with our previous results collected for the DODA⁺ salts of Keplerates [36,37] and of similar salts obtained with the anisotropic POM $[\text{K}_2\text{Na}_x\text{Li}_y\text{H}_z\{\text{Mo}_4\text{O}_4\text{S}_4(\text{OH})_2(\text{H}_2\text{O})_3\}_2(\text{P}_8\text{W}_{48}\text{O}_{184})]^{(34-x-y-z)-}$ [38]. In the former case, the larger number and the vicinity of alkyl chains of the DODA⁺ cations within the solid favor the interdigitation of the alkyl chains driven by van der waals interactions. In the second case, the anisotropic shape of the POM associated with the cationic character of its cavity promotes the localization of the cations on the anionic ring of the P₈W₄₈-POM. This favors the closeness of the cations and thus the van der Waals interactions between alkyl chains and therefore the organization within the solid and the liquid crystal phase. This strategy to combine POMs and very simple cations like alkylimidazolium or DODA⁺

cation then appears efficient if we can induce interaction between alkyl chains especially by forcing the cations to be close by using a limited surface for the POM or by using cations bearing several alkyl chains like DODA⁺ cations.

Acknowledgments

We acknowledge the Centre National de la Recherche Scientifique (CNRS), the Ministère de l'Éducation Nationale de l'Enseignement Supérieur et de la Recherche (MENESR) and the University of Versailles Saint Quentin for their financial support. SF gratefully acknowledges the "Institut Universitaire de France, IUF" for financial support. CP and LG gratefully acknowledges the financial support from the Swiss National Science Foundation.

Author Contributions

The syntheses and characterizations were performed by NW, WS and AH. The study of the liquid crystals phases by TD-POM, DSC and SA-XRD were ensured by ET, LG and KLB. CP contributed for the interpretation of the liquid crystal data. EC and DN contributed to this work as supervisors of NW and WS. SF ensured the coordination of this work, the co-supervision of NW, WS and AH and the FT-IR experiments with temperature.

Conflicts of Interest

The authors declare no conflict of interest.

References

1. Binnemans, K.; Gorller-Walrand, C. Lanthanide-Containing Liquid Crystals and Surfactants. *Chem. Rev.* **2002**, *102*, 2303–2346.
2. Vila-Nadal, L.; Mitchell, S.G.; Markov, S.; Busche, C.; Georgiev, V.; Asenov, A.; Cronin, L. Towards Polyoxometalate-Cluster-Based Nano-Electronics. *Chem.-Eur. J.* **2013**, *19*, 16502–16511.
3. Evangelisti, F.; Guttinger, R.; More, R.; Lubner, S.; Patzke, G.R. Closer to Photosystem II: A Co₄O₄ Cubane Catalyst with Flexible Ligand Architecture. *J. Am. Chem. Soc.* **2013**, *135*, 18734–18737.
4. Carraro, M.; Modugno, G.; Zamolo, V.; Bonchio, M.; Fabbretti, E. Polyoxometalate-Based Conjugates for Biological Targeting. *J. Biol. Inorg. Chem.* **2014**, *19*, S406–S406.
5. Ibrahim, M.; Xiang, Y.X.; Bassil, B.S.; Lan, Y.H.; Powell, A.K.; de Oiveira, P.; Keita, B.; Kortz, U. Synthesis, Magnetism, and Electrochemistry of the Ni₁₄ and Ni₅-Containing Heteropolytungstates [Ni₁₄(OH)₆(H₂O)₁₀(HPO₄)₄(P₂W₁₅O₅₆)₄]³⁴⁻ and [Ni₅(OH)₄(H₂O)₄(β-GeW₉O₃₄)(β-GeW₈O₃₀(OH))]¹³⁻. *Inorg. Chem.* **2013**, *52*, 8399–8408.
6. Absillis, G.; Parac-Vogt, T.N. Peptide Bond Hydrolysis Catalyzed by the Wells–Dawson [Zr(α₂-P₂W₁₇O₆₁)₂] Polyoxometalate. *Inorg. Chem.* **2012**, *51*, 9902–9910.

7. Riflade, B.; Oble, J.; Chenneberg, L.; Derat, E.; Hasenknopf, B.; Lacote, E.; Thorimbert, S. Hybrid Polyoxometalate Palladacycles: DFT Study and Application to the Heck Reaction. *Tetrahedron* **2013**, *69*, 5772–5779.
8. Wang, Y.F.; Weinstock, I.A. Polyoxometalate-Decorated Nanoparticles. *Chem. Soc. Rev.* **2012**, *41*, 7479–7496.
9. Rickert, P.G.; Antonio, M.R.; Firestone, M.A.; Kubatko, K.-A.; Szreder, T.; Wishart, J.F.; Dietz, M.L. Tetraalkylphosphonium Polyoxometalate Ionic Liquids: Novel, Organic-Inorganic Hybrid Materials. *J. Phys. Chem. B* **2007**, *111*, 4685–4692.
10. Lin, X.K.; Li, W.; Zhang, J.; Sun, H.; Yan, Y.; Wu, L.X. Thermotropic Liquid Crystals of a Non-Mesogenic Group Bearing Surfactant-Encapsulated Polyoxometalate Complexes. *Langmuir* **2010**, *26*, 13201–13209.
11. Yin, S.Y.; Sun, H.; Yan, Y.; Li, W.; Wu, L.X. Hydrogen-Bonding-Induced Supramolecular Liquid Crystals and Luminescent Properties of Europium-Substituted Polyoxometalate Hybrids. *J. Phys. Chem. B* **2009**, *113*, 2355–2364.
12. Yin, S.Y.; Li, W.; Wang, J.F.; Wu, L.X. Mesomorphic Structures of Protonated Surfactant-Encapsulated Polyoxometalate Complexes. *J. Phys. Chem. B* **2008**, *112*, 3983–3988.
13. Li, W.; Yin, S.Y.; Wang, J.F.; Wu, L.X. Tuning Mesophase of Ammonium Amphiphile-Encapsulated Polyoxometalate Complexes through Changing Component Structure. *Chem. Mater.* **2008**, *20*, 514–522.
14. Li, W.; Bu, W.F.; Li, H.L.; Wu, L.X.; Li, M. A Surfactant-Encapsulated Polyoxometalate Complex towards a Thermotropic Liquid Crystal. *Chem. Commun.* **2005**, 3785–3787.
15. Li, B.; Zhang, J.; Wang, S.; Li, W.; Wu, L.X. Nematic Ion-Clustomesogens from Surfactant-Encapsulated Polyoxometalate Assemblies. *Eur. J. Inorg. Chem.* **2013**, 1869–1875.
16. Jiang, Y.X.; Liu, S.X.; Zhang, J.; Wu, L.X. Phase Modulation of Thermotropic Liquid Crystals of Tetra-*n*-Alkylammonium Polyoxometalate Ionic Complexes. *Dalton Trans.* **2013**, *42*, 7643–7650.
17. Yin, S.Y.; Sun, H.; Yan, Y.; Zhang, H.; Li, W.; Wu, L.X. Self-Assembly and Supramolecular Liquid Crystals based on Organic Cation Encapsulated Polyoxometalate Hybrid Reverse Micelles and Pyridine Derivatives. *J. Colloid Interface Sci.* **2011**, *361*, 548–555.
18. Müller, A.; Gouzerh, P. Capsules with Highly Active Pores and Interiors: Versatile Platforms at the Nanoscale. *Chem.-Eur. J.* **2014**, *20*, 4862–4873.
19. Müller, A.; Gouzerh, P. From Linking of Metal-Oxide Building Blocks in a Dynamic Library to Giant Clusters with Unique Properties and Towards Adaptive Chemistry. *Chem. Soc. Rev.* **2012**, *41*, 7431–7463.
20. Kögerler, P.; Tsukerblat, B.; Müller, A. Structure-Related Frustrated Magnetism of Nanosized Polyoxometalates: Aesthetics and Properties in Harmony. *Dalton Trans.* **2010**, *39*, 21–36.
21. Botar, B.; Kögerler, P.; Müller, A.; Garcia-Serres, R.; Hill, C.L. Ferrimagnetically Ordered Nanosized Polyoxomolybdate-Based Cluster Spheres. *Chem. Commun.* **2005**, 5621–5623.
22. Rezaeifard, A.; Haddad, R.; Jafarpour, M.; Hakimi, M. Catalytic Epoxidation Activity of Keplerate Polyoxomolybdate Nanoball toward Aqueous Suspension of Olefins under Mild Aerobic Conditions. *J. Am. Chem. Soc.* **2013**, *135*, 10036–10039.

23. Kopilevich, S.; Gil, A.; Garcia-Rates, M.; Bonet-Avalos, J.; Bo, C.; Müller, A.; Weinstock, I.A. Catalysis in a Porous Molecular Capsule: Activation by Regulated Access to Sixty Metal Centers Spanning a Truncated Icosahedron. *J. Am. Chem. Soc.* **2012**, *134*, 13082–13088.
24. Ostroushko, A.A.; Grzhegorzhevskii, K.V. Electric Conductivity of Nanocluster Polyoxomolybdates in the Solid State and Solutions. *Russ. J. Phys. Chem. A* **2014**, *88*, 1008–1011.
25. Zhou, Y.S.; Shi, Z.H.; Zhang, L.J.; ul Hassan, S.; Qu, N.N. Notable Third-Order Optical Nonlinearities of a Keplerate-Type Polyoxometalate in Solution and in Thin Films of PMMA. *Appl. Phys. A* **2013**, *113*, 563–568.
26. Zhang, L.J.; Shi, Z.H.; Zhang, L.H.; Zhou, Y.S.; ul Hassan, S. Fabrication and Optical Nonlinearities of Ultrathin Composite Films Incorporating a Keplerate Type Polyoxometalate. *Mater. Lett.* **2012**, *86*, 62–64.
27. Besson, C.; Schmitz, S.; Capella, K.M.; Kopilevich, S.; Weinstock, I.A.; Kögerler, P. A Regioselective Huisgen Reaction inside a Keplerate Polyoxomolybdate Nanoreactor. *Dalton Trans.* **2012**, *41*, 9852–9854.
28. Zhang, Q.; He, L.P.; Wang, H.; Zhang, C.; Liu, W.S.; Bu, W.F. Star-Like Supramolecular Polymers Fabricated by a Keplerate Cluster with Cationic Terminated Polymers and their Self-Assembly into Vesicles. *Chem. Commun.* **2012**, *48*, 7067–7069.
29. Caruso, F.; Kurth, D.G.; Volkmer, D.; Koop, M.J.; Müller, A. Ultrathin Molybdenum Polyoxometalate-Polyelectrolyte Multilayer Films. *Langmuir* **1998**, *14*, 3462–3465.
30. Cazacu, A.; Mihai, S.; Nasr, G.; Mahon, E.; van der Lee, A.; Meffre, A.; Barboiu, M. Lipophilic Polyoxomolybdate Nanocapsules in Constitutional Dynamic Hybrid Materials. *Inorg. Chim. Acta* **2010**, *363*, 4214–4219.
31. Kurth, D.G.; Volkmer, D.; Ruttorf, M.; Richter, B.; Müller, A. Ultrathin Composite Films Incorporating the Nanoporous Isopolyoxomolybdate "Keplerate" $(\text{NH}_4)_{42}[\text{Mo}_{132}\text{O}_{372}(\text{CH}_3\text{COO})_{30}(\text{H}_2\text{O})_{72}]$. *Chem. Mater.* **2000**, *12*, 2829–2831.
32. Kurth, D.G.; Lehmann, P.; Volkmer, D.; Müller, A.; Schwahn, D. Biologically Inspired Polyoxometalate-Surfactant Composite Materials. Investigations on the Structures of Discrete, Surfactant-Encapsulated Clusters, Monolayers, and Langmuir-Blodgett Films of $(\text{DODA})_{40}(\text{NH}_4)_2(\text{H}_2\text{O})_n[\text{Mo}_{132}\text{O}_{372}(\text{CH}_3\text{CO}_2)_{30}(\text{H}_2\text{O})_{72}]$. *Dalton Trans.* **2000**, 3989–3998.
33. Kurth, D.G.; Lehmann, P.; Volkmer, D.; Colfen, H.; Koop, M.J.; Müller, A.; Du Chesne, A. Surfactant-Encapsulated Clusters (SECs): $(\text{DODA})_{20}(\text{NH}_4)[\text{H}_3\text{Mo}_{57}\text{V}_6(\text{NO})_6\text{O}_{183}(\text{H}_2\text{O})_{18}]$, a Case Study. *Chem.-Eur. J.* **2000**, *6*, 385–393.
34. Volkmer, D.; Du Chesne, A.; Kurth, D.G.; Schnablegger, H.; Lehmann, P.; Koop, M.J.; Müller, A. Toward Nanodevices: Synthesis and Characterization of the Nanoporous Surfactant-Encapsulated Keplerate $(\text{DODA})_{40}(\text{NH}_4)_2(\text{H}_2\text{O})_n[\text{Mo}_{132}\text{O}_{372}(\text{CH}_3\text{CO}_2)_{30}(\text{H}_2\text{O})_{72}]$. *J. Am. Chem. Soc.* **2000**, *122*, 1995–1998.
35. Clemente-Leon, M.; Ito, T.; Yashiro, H.; Yamase, T. Two-Dimensional Array of Polyoxomolybdate Nanoball Constructed by Langmuir-Blodgett Semiamphiphilic Method. *Chem. Mater.* **2007**, *19*, 2589–2594.

36. Floquet, S.; Terazzi, E.; Korenev, V.S.; Hijazi, A.; Guénée, L.; Cadot, E. Layered Ionic Liquid-Crystalline Organisations Built from Nano-Capsules $[\text{Mo}_{132}\text{O}_{312}\text{S}_{60}(\text{SO}_4)_x(\text{H}_2\text{O})_{(132-2x)}]^{(12+2x)-}$ and DODA⁺ cations. *Liq. Cryst.* **2014**, *41*, 1000–1007.
37. Floquet, S.; Terazzi, E.; Hijazi, A.; Guénée, L.; Piguet, C.; Cadot, E. Evidence of Ionic Liquid Crystal Properties for a DODA⁺ Salt of the Keplerate $[\text{Mo}_{132}\text{O}_{372}(\text{CH}_3\text{COO})_{30}(\text{H}_2\text{O})_{72}]^{42-}$. *New J. Chem.* **2012**, *36*, 865–868.
38. Watfa, N.; Floquet, S.; Terazzi, E.; Haouas, M.; Salomon, W.; Korenev, V.S.; Taulelle, F.; Guénée, L.; Hijazi, A.; Naoufal, D.; *et.al.* Synthesis, Characterization, and Tuning of the Liquid Crystal Properties of Ionic Materials based on the Cyclic Polyoxothiometalate $[\{\text{Mo}_4\text{O}_4\text{S}_4(\text{H}_2\text{O})_3(\text{OH})_2\}_2(\text{P}_8\text{W}_{48}\text{O}_{184})]^{36-}$. *Soft Matter* **2015**, *11*, 1087–1099.
39. Watfa, N.; Melgar, D.; Haouas, M.; Taulelle, F.; Hijazi, A.; Naoufal, D.; Bonet Avalos, J.; Floquet, S.; Bo, C.; Cadot, E. Hydrophobic Effect as Driving Force for Host-Guest Chemistry of a Multireceptor Keplerate-Type Capsule. *J. Am. Chem. Soc.* **2015**, *137*, 5845–5851.
40. Dutronc, T.; Terazzi, E.; Guénée, L.; Buchwalder, K.L.; Spoerri, A.; Emery, D.; Mareda, J.; Floquet, S.; Piguet, C. Enthalpy-Entropy Compensation Combined with Cohesive Free-Energy Densities for Tuning the Melting Temperatures of Cyanobiphenyl Derivatives. *Chem.-Eur. J.* **2013**, *19*, 8447–8456.
41. Deschenaux, R.; Donnio, B.; Guillon, D. Liquid-Crystalline Fullerodendrimers. *New J. Chem.* **2007**, *31*, 1064–1073.
42. Müller, A.; Krickemeyer, E.; Bögge, H.; Schmidtman, M.; Peters, F. Organizational Forms of Matter: An Inorganic Super Fullerene and Keplerate based on Molybdenum Oxide. *Angew. Chem.* **1998**, *37*, 3359–3363.

© 2015 by the authors; licensee MDPI, Basel, Switzerland. This article is an open access article distributed under the terms and conditions of the Creative Commons Attribution license (<http://creativecommons.org/licenses/by/4.0/>).